

X-ray scattering from a plane parallel slab using radiation transfer considerations*

Stanislav Stoupin[†]

Cornell High Energy Synchrotron Source, Cornell University, Ithaca, NY 14853, USA

X-ray scattering power of a plane parallel homogeneous slab of material is derived using radiation intensity transfer equations. The scattering power scales with the ratio of the scattering coefficient of interest to the total attenuation coefficient. The results can be used to guide the choice of slab thickness, scattering geometry and photon energy to maximize scattering power in both elastic and inelastic X-ray scattering experiments.

I. INTRODUCTION

The optimal choice of photon energy and sample thickness in X-ray scattering experiments deserves clarifications based on clear understanding of radiation transfer in specimens of finite thickness. The well-known practical requirement (“rule of thumb”) for optimization of scattered intensity in transmission through a sample states that the optimal sample thickness should be approximately equal to the radiation attenuation length Λ :

$$T_{opt} \simeq \gamma_0 / \mu, \quad (1)$$

where $\mu = 1/\Lambda$ is the total attenuation coefficient [11] and γ_0 is the direction cosine for the X-ray beam incident on the sample (the angle between the wavevector of the incident beam and the inward normal to the sample surface). Intuitively it is clear that to maximize scattering in reflection from the sample its thickness should be $T \gtrsim T_{opt}$. The basic sample geometry is that of the infinite parallel slab of material as shown in Fig. 1. The direction cosine of the incident beam $\gamma_0 = \cos \alpha$ and the direction cosine of the scattered beam is $\gamma_s = \cos(\alpha + \theta)$, where α is the incidence angle and θ is the scattering angle. By definition, $\gamma_0 > 0$, $\gamma_s > 0$ for the transmission geometry and $\gamma_s < 0$ for the reflection geometry.

Some textbooks provide additional relevant details [1–3]. For example, [2] includes expressions for the scattering power

(fraction of photons scattered) from a parallel slab in the symmetric ($\gamma_0 = |\gamma_s|$) transmission and reflection geometries. A general recipe for the calculation of the absorption correction (here termed as attenuation correction) is given by International Tables for Crystallography [4].

$$A = \frac{1}{V} \int \exp(-\mu\Gamma) dV, \quad (2)$$

where the integral is taken over the sample volume V exposed to X-rays and Γ is the path length of the X-ray beam in the sample (the sum of the path lengths for the penetrating incident beam and the scattered beam). Several expressions for special cases of the parallel slab geometry are tabulated [4]. Meanwhile, the absorption correction for the parallel slab in case of arbitrary angle of incidence and arbitrary scattering angle can be readily derived using Eq. (2) (e.g., [1]).

In this work it is shown that consideration of intensity radiation transfer (Darwin-Hamilton equations) in the plane parallel slab while neglecting effects of multiple scattering leads to the same expressions as the ones derived using Eq. (2). The solutions are expressed as functions of the momentum transfer for X-rays. The dependence of the scattering power on the momentum transfer due to the parallel slab geometry is analyzed and illustrated. Finally, energy dependence of the leading term, the scattering-attenuation contrast (the ratio of the scattering coefficient of interest σ to the attenuation coefficient) is illustrated assuming isotropic (average) cross sections, which can guide the choice of optimal photon energy. While the choice of photon energy and the slab thickness can maximize the contrast and thus optimize the scattering power, the contrast has to remain small ($\sigma_0/\mu \ll 1$) to avoid multiple scattering effects.

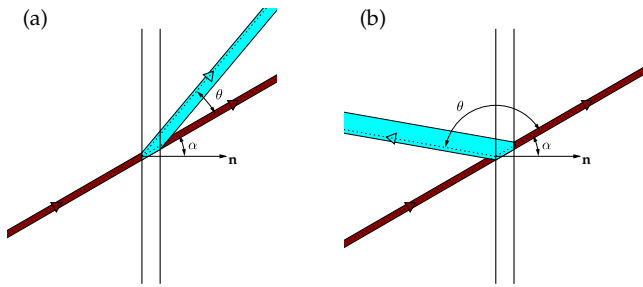


FIG. 1: Scattering from the parallel slab in transmission geometry (a) and in reflection geometry (b).

II. ATTENUATION CORRECTION

The path of the X-ray beam in the parallel slab is

$$\Gamma = \begin{cases} \frac{z}{\gamma_0} + \frac{(T-z)}{\gamma_s}, & \text{transmission } (\gamma_s > 0) \\ \frac{z}{\gamma_0} - \frac{z}{\gamma_s}, & \text{reflection } (\gamma_s < 0), \end{cases} \quad (3)$$

where T is the slab thickness and z is the variable depth at which scattering event occurs. For the photon energies of practical importance in X-ray scattering experiments (e.g., $E \lesssim 100$ keV) the non-negligible attenuation processes are photoabsorption, elastic (Rayleigh) and inelastic (Compton) scattering. A general case of scattering can be considered

*Submitted to J. Appl. Cryst.

[†]Electronic address: sstoupin@cornell.edu

where the scattered photon can lose a fraction of its energy (i.e., inelastic scattering). The scattered beam of interest, propagating in a direction defined by γ_s will encounter attenuation coefficient $\mu_s(E_s)$, which can be different from that of the incident beam $\mu_0(E_0)$. Using Eqs. 2 and 3 for the parallel slab one can readily obtain for the scattering power:

$$s = \sigma_0 \frac{T}{\gamma_0} A = \begin{cases} \frac{\sigma_0}{\mu_s b - \mu_0} e^{-\mu_0 T / \gamma_0} \left[1 - e^{-(\mu_s b - \mu_0) T / \gamma_0} \right], & \gamma_s > 0, \\ \frac{\sigma_0}{\mu_0 - \mu_s b} \left[1 - e^{-(\mu_0 - \mu_s b) T / \gamma_0} \right], & \gamma_s < 0, \end{cases} \quad (4)$$

where $b = \gamma_0 / \gamma_s$ is the asymmetry ratio of the scattering geometry and $\sigma_0 = \sigma_0^s(E_0)$ is the scattering coefficient (per unit thickness, similarly to μ) of the incident beam with photon energy E_0 into the scattering channel with photon energy E_s .

The attenuation correction does not take into account effects of multiple scattering, which can be split into two categories. If the slab is a single crystal in the Bragg diffraction condition (elastic scattering), multiply scattered photons can add up coherently such that the resulting scattering direction is well defined (to the extent defined by the divergence/bandwidth of the incident beam and the perfection of the crystal structure). A detector placed to capture photons scattered in this direction will probe the corresponding momentum transfer. On the other hand, for any slab of material the other type of multiple scattering exists where the photons traversing the slab exhibit a few different momentum transfers (two as the strongest contribution) prior to arriving at the detector. For these photons the directional placement of the detector does not correspond to a particular momentum transfer. Therefore, multiple scattering of this second type should be avoided in X-ray scattering experiments as long as resolving the momentum transfer remains of primary interest. Dedicated studies show that such multiple scattering (both elastic and inelastic) is non-negligible at photon energies of $E \gtrsim 30$ keV for materials of low atomic numbers (e.g., [5, 6]).

III. SIMPLIFIED RADIATION TRANSFER EQUATIONS AND THEIR SOLUTIONS

Darwin-Hamilton equations [7–9] describe radiation intensity transfer in X-ray diffraction from a mosaic crystal. In the Bragg diffraction condition where multiple scattering of the first type is expected to be the dominant scattering mechanism, the contribution of the second type of multiple-scattering is neglected. The notion of a crystal structure is specific to the formulation of the scattering coefficient σ . Therefore, assuming that the second type of multiple scattering is avoided and that wave mixing/interference effects are negligible the Darwin-Hamilton equations can be generalized to describe radiation transfer in X-ray scattering experiments. The generalized equations are:

$$\frac{dI_0(E_0)}{dt} = -\frac{\mu(E_0)}{\gamma_0} I_0(E_0) + \frac{\sigma_s^0(E_s)}{|\gamma_s|} I_s(E_s), \quad (5)$$

$$\frac{dI_s(E_s)}{dt} = -\frac{\mu(E_s)}{\gamma_s} I_s(E_s) \pm \frac{\sigma_0^s(E_0)}{\gamma_0} I_0(E_0), \quad (6)$$

where I_0 and I_s are the intensities of the incident and scattered beams respectively, t is the coordinate along the inward normal to the slab surface, γ_0 and γ_s are the direction cosines for the transmitted and scattered beams respectively. The upper sign corresponds to the beam scattered in transmission through the slab and the lower sign corresponds to the beam scattered in the reflection geometry.

Unlike the original Darwin-Hamilton equations, which describe the elastic process, scattering can occur at a different photon energy E_s (i.e., inelastic scattering process). The scattering coefficient of interest is $\sigma_0^s(E_0)$ corresponds to scattering of the primary beam with photon energy E_0 into the scattering channel with a photon energy E_s . Similarly, re-scattering of the scattered beam back into the primary beam is described with $\sigma_s^0(E_s)$. In general, μ , σ and I_s are functions of the direction of propagation, which is omitted from the notation for brevity. Aside from the case of Bragg diffraction in crystalline samples a common situation in X-ray scattering experiments is $I_s \ll I_0$, while the scattering power of interest is relatively weak $\sigma_0^s \approx \sigma_s^0 \ll \mu$. In these conditions, the last term in Eq. 5, $\frac{\sigma_s^0(E_s)}{|\gamma_s|} I_s(E_s)$ is a second order quantity (aside from cases of extreme grazing emergence $|\gamma_s| \simeq 0$ not considered here). In other words, an assumption is made that the multiple scattering of the first type is small. The first equation resolves as the well known Beer-Lambert law

$$I_0(E_0) = I_0^0 \exp[-\mu(E_0)t/\gamma_0], \quad (7)$$

where I_0^0 is the intensity of the incident beam at the entrance surface. Thus the radiation transfer equations become decoupled. Upon substitution of Eq. (7) the equation for the scattered intensity is

$$\frac{dI_s}{dt} = -\frac{\mu_s}{\gamma_s} I_s \pm \frac{\sigma_0 I_0^0}{\gamma_0} \exp(-\mu_0 t / \gamma_0). \quad (8)$$

Here, for brevity $I_s = I_s(E_s)$, $\sigma_0 = \sigma_0^s(E_0)$, $\mu_s = \mu(E_s)$ and $\mu_0 = \mu(E_0)$.

Equation (8) can be easily solved analytically using appropriate boundary conditions. For the transmission case $I_s|_{t=0} = 0$ and the scattering power $s = I_s|_{t=T} / I_0^0$ is found for the slab of thickness T . For the reflection case $I_s|_{t=T} = 0$ and the scattering power $s = I_s|_{t=0} / I_0^0$ is found at the entrance surface. It is easy to see that the resulting expressions are the same as those derived in the previous section (Eq. (4)).

IV. ANALYSIS OF SOLUTIONS, SPECIAL CASES

A. Transmission geometry

In the transmission geometry an optimal thickness exists where the scattered intensity attains its maximum value. The

optimal thickness and the scattering power for this thickness are

$$T_{opt} = \frac{\gamma_0 \ln[b\mu_s/\mu_0]}{\mu_s b - \mu_0}, \quad (9)$$

$$s_{opt} = \frac{\sigma_0}{b\mu_s} \exp\left[-\frac{\mu_0 \ln[b\mu_s/\mu_0]}{\mu_s b - \mu_0}\right]. \quad (10)$$

For experiments where the elastically scattered component is detected (e.g., small angle or wide angle X-ray scattering (SAXS/WAXS)) the above expressions can be simplified by letting $\mu_0 = \mu_s = \mu$. Also, the subscript is omitted in the notation for the scattering coefficient $\sigma_0 = \sigma$. The scattering power is

$$s = \frac{\sigma}{(b-1)\mu} e^{-\mu T/\gamma_0} \left[1 - e^{-\mu(b-1)T/\gamma_0}\right]. \quad (11)$$

Eqs. 9 and 10 are reduced to:

$$T_{opt} = \frac{\gamma_0 \ln b}{(b-1)\mu}, \quad (12)$$

$$s_{opt} = \frac{\sigma}{b\mu} \exp\left[-\frac{\ln b}{b-1}\right]. \quad (13)$$

These simplified expressions (Eqs. 11, 12 and 13) are also valid for nonresonant inelastic experiments, where $\mu(E)$ is a smooth function and the scattered intensity is measured selectively using an energy discriminating detector (including use of a crystal analyzer) at a reasonably small energy offset, such that $\mu_s \simeq \mu_0 = \mu$. For the symmetric scattering geometry ($b = 1$), and in the regime of small angle scattering ($\gamma_0 \simeq \gamma_s$) Eqs. 11, 12 and 13 are reduced to the well known expressions:

$$s = \frac{\sigma T}{\gamma_0} e^{-\mu T/\gamma_0}, \quad (14)$$

$$T_{opt} = \frac{\gamma_0}{\mu}, \quad (15)$$

$$s_{opt} = \frac{\sigma}{\mu} e^{-1}. \quad (16)$$

B. Reflection geometry

For the elastic and nonresonant inelastic experiments as described in the previous subsection ($\mu_0 = \mu_s = \mu$, $\sigma_0 = \sigma$):

$$s = \frac{\sigma}{(1-b)\mu} \left[1 - e^{-\mu(1-b)T/\gamma_0}\right], \quad (17)$$

which is reduced to

$$s = \frac{\sigma}{2\mu} \left[1 - e^{-2\mu T/\gamma_0}\right], \quad (18)$$

for the symmetric scattering geometry ($b = -1$). From Eqs. (14) and (18) it follows that in the case of small attenuation $\mu T/\gamma_0 \ll 1$ the scattering power is $s \simeq \frac{\sigma T}{\gamma_0}$, i. e. proportional to the effective slab thickness T/γ_0 in both transmission and reflection cases. Otherwise, it is proportional to the ratio σ/μ , which will be further referred to as scattering-attenuation contrast.

V. DEPENDENCE ON THE MOMENTUM TRANSFER FOR X-RAYS

For X-rays the scattering angle θ is conveniently related to the modulus of momentum transfer $Q = 2k_0 \sin(\theta/2)$. The change in the modulus of the wavevector k_0 upon scattering is either zero (elastic scattering) or very small (quasielastic scattering). Assuming normal incidence of X-rays ($\gamma_0=1$) the exit angle for the scattered beam with respect to the normal becomes equal to the scattering angle. The direction cosine of the scattered beam is

$$\gamma_s = 1 - 2q^2, \quad (19)$$

where $q = \frac{Q}{2k_0} = \sin(\theta/2)$ is the reduced momentum transfer. In the transmission geometry $0 \leq q < 1.0/\sqrt{2}$. The solution for the scattering power Eqs. (11) can be expressed as a function of the reduced momentum transfer.

$$s(q) = \frac{\sigma(q)}{\mu(q)} \frac{e^{-\mu(q)T}}{f(q)} \left[1 - e^{-\mu(q)Tf(q)}\right], \quad (20)$$

where

$$f(q) = \frac{2q^2}{1 - 2q^2} \quad (21)$$

In the reflection geometry ($1/\sqrt{2} < q \leq 1$) the dependence on the momentum transfer can be derived similarly. Assuming normal incidence $\gamma_0 = 1$ and using Eq. (19), Eq.(17) can be written as

$$s(q) = \frac{\sigma(q)}{\mu(q)} \frac{1}{f(q)} \left[e^{\mu(q)Tf(q)} - 1\right] \quad (22)$$

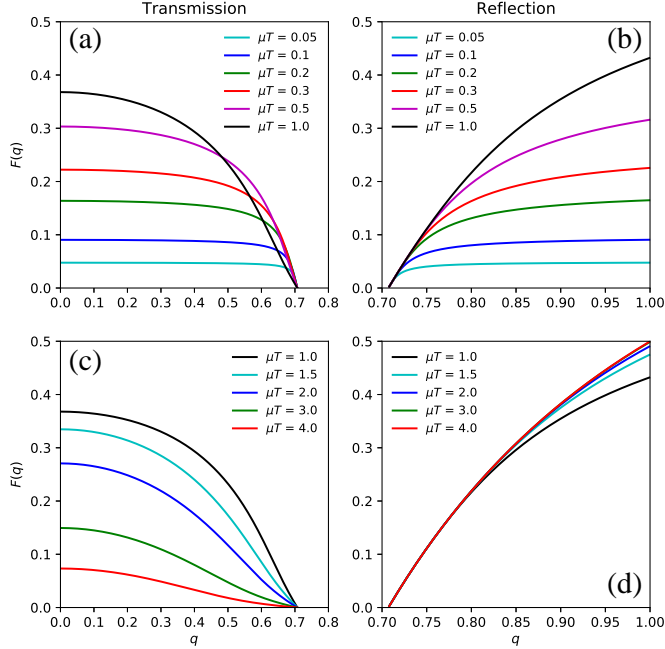
The leading term in the expressions for the scattering power is the scattering-attenuation contrast σ/μ . The scattering geometry defines the measured direction-dependent fraction of the scattering-attenuation contrast. If the latter is denoted as $F(q)$ the scattering power is

$$s = \frac{\sigma(q)}{\mu(q)} F(q), \quad (23)$$

$$F(q) = \begin{cases} \frac{e^{-\mu(q)T}}{f(q)} \left[1 - e^{-\mu(q)Tf(q)}\right], & \text{if } 0 \leq q < 1/\sqrt{2}, \\ \frac{1}{f(q)} \left[e^{\mu(q)Tf(q)} - 1\right], & \text{if } 1/\sqrt{2} < q \leq 1 \end{cases}$$

The geometric factor $F(q)$ is plotted in Fig. 2 for different values of slab thickness in both transmission and reflection

FIG. 2: Geometric factor $F(q)$ (case of normal incidence) for different values of slab thickness (μT): (a) transmission geometry, $0.05 \leq \mu T \leq 1.0$; (b) reflection geometry, $0.05 \leq \mu T \leq 1.0$; (c) transmission geometry, $1.0 \leq \mu T \leq 4.0$; (d) reflection geometry, $1.0 \leq \mu T \leq 4.0$. The maximum value of $F(q)$ ($F(0)$ for transmission and $F(1)$ for reflection) is monotonically increasing with μT for (a) and (d) and decreasing for (c).



geometries. The dependence $\mu(q)$ is not considered, which corresponds to a case where total attenuation is dominated by isotropic processes. $F(q)$ is the thickness and momentum-transfer-dependent correction to the scattering power. The correction is non-negligible in general and of particular importance in the regime of wide angle scattering for $\mu T \gtrsim 1$. $F(q)$ normalized to its maximum value exhibits different shapes with variation in μT (see Appendix A).

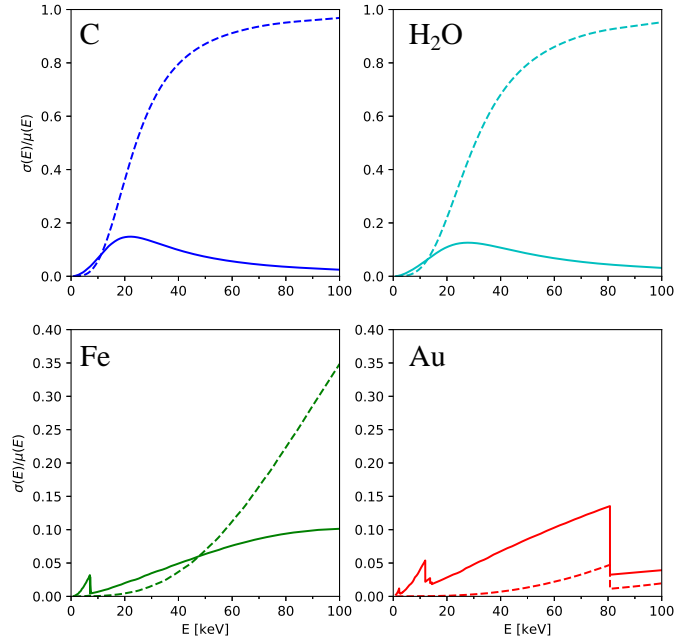
In the transmission geometry the geometric factor $F(q)$ attains its maximum values e^{-1} in the regime of small angle scattering ($q \approx 0$). In the reflection geometry $F(q)$ attains its maximum value $1/2$ at backscattering ($q = 1$) for an infinitely thick slab converging to this value rapidly for $\mu T \gtrsim 2$ (see Fig.2(d)).

Analysis in the more general case of arbitrary angle of incidence is given in Appendix B. Increase in $F(q)$ beyond the limiting values e^{-1} and $1/2$ can be obtained by choice of α . This can lead to an enhancement in the measured scattered intensity as long as the scattering geometry remains practical and the resulting scattered beam is fully intercepted by the detector.

VI. ON THE SCATTERING-ATTENUATION CONTRAST

For the special cases discussed above, small angle scattering and backscattering, the variation in the geometric factor with q can be neglected. The optimal scattering power is defined only by the scattering-attenuation contrast. It is informative to explore dependence of the scattering-attenuation contrast on the photon energy. The contrast is plotted in Fig.VI for several representative compounds using values of the scattering and attenuation cross sections taken from XCOM database [10]. The solid curves represent coherent (elastic) scattering and the dashed curves represent incoherent (inelastic) scattering. For illustrative purposes it is assumed that the scattering is isotropic. The focus is on comparison of fractions of coherently and incoherently scattered intensity, which gives an insight on the optimal choice of photon energy in non-resonant X-ray scattering experiments.

FIG. 3: Scattering-attenuation contrast $\sigma(E)/\mu(E)$ using XCOM database for selected compounds. Solid lines correspond to coherent (elastic) scattering and dashed lines correspond to incoherent (inelastic) scattering.



For compounds of low atomic numbers such as carbon and water the elastic component dominates up to about 10-15 keV (as shown in Fig.VI). Above these popular energies the enhancement in inelastic scattering is rather significant, which makes selective detection of elastic scattering more difficult. If, however, inelastic scattering is suppressed using energy discrimination, the elastic component is maximized at photon energies of about 20-30 keV. For high-Z compounds (Fe and Au shown in Fig.VI) the scattering-attenuation contrasts are monotonically increasing with photon energy (aside from transitions due to the photoabsorption edges). For Fe the

inelastic component begins to dominate at ≈ 50 keV while for Au the elastic component remains dominant up to 100 keV and beyond. It is clear that for all compounds inelastic scattering experiments should benefit from the choice of higher photon energies due to enhancement in the corresponding scattering-attenuation contrast (shown by the dashed lines in Fig. VI).

It should be noted that in the practical range of photon energies considered here (up to 100 keV) the scattering-attenuation contrast for elastic X-ray scattering remains small for either low-Z or high-Z compounds ($\sigma/\mu \lesssim 0.2$). On the contrary, the scattering-attenuation contrast for inelastic X-ray scattering from low-Z materials gradually approaches unity at higher photon energies, thus violating the approximation of negligible multiple scattering. Finally, it is noted that practical calculation of scattered intensity measured in an experiment should include considerations of the scattering cross section of interest (from which $\sigma(q)$ is derived), polarization effects and detector/analyzer acceptances.

VII. CONCLUSIONS

In conclusion, X-ray scattering power of a plane parallel homogeneous slab of material was derived using radiation transfer considerations. Arbitrary angles of incidence and emergence were considered using an analogy with reflection geometry of an asymmetric crystal. In the case of small angle scattering in transmission through the slab the expressions are reduced to the well known "rule of thumb" where the optimal sample thickness is inversely proportional to the total attenuation coefficient. In the general case, the parallel slab geometry yields direction-dependent corrections to scattered intensity. These corrections are essential in the regime of wide-angle scattering for samples with thickness approximately equal to or greater than the optimal thickness. The correction was formulated as momentum transfer-dependent geometric factor. The scattering power is described as the product of the photon energy-dependent scattering-attenuation contrast and the derived geometric factor. The dependence of the scattering-attenuation contrast on the photon energy was explored for both elastic and inelastic scattering, assuming isotropic processes for simplicity. The results can be used in finding optimal experimental conditions to enhance weak scattering (both elastic and inelastic) of interest for samples with plane parallel slab geometry.

Acknowledgments

J.P.C. Ruff, D.M. Smilgies and C. Franck are acknowledged for helpful discussions. This work is based upon research conducted at the Cornell High Energy Synchrotron Source (CHESS) which is supported by the National Science Foundation under award DMR-1332208.

Appendix A: Case of normal incidence ($\gamma_0 = 1$): Normalized geometric factor $F(q)$.

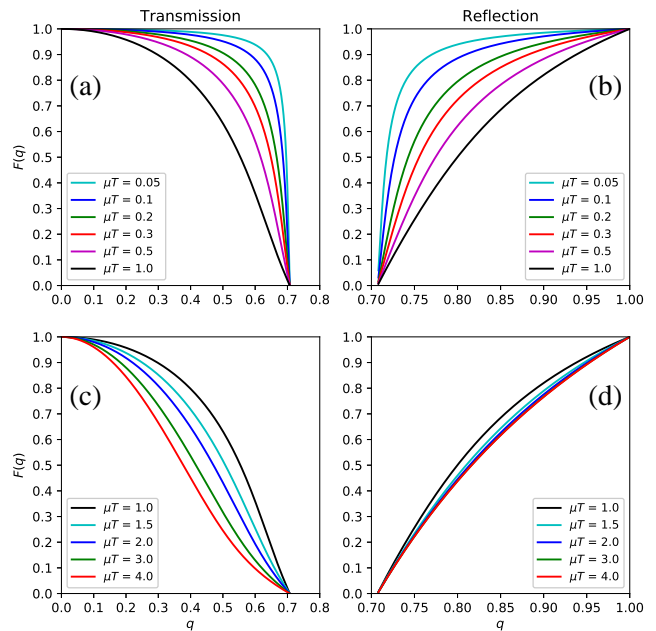


FIG. 4: Geometric factor $F(q)$ normalized by its maximum value (normal incidence) plotted for different values of slab thickness (μT): (a) transmission geometry, $0.05 \leq \mu T \leq 1.0$; (b) reflection geometry, $0.05 \leq \mu T \leq 1.0$; (c) transmission geometry, $1.0 \leq \mu T \leq 4.0$; (d) reflection geometry, $1.0 \leq \mu T \leq 4.0$. The maximum value of $F(q)$ ($F(0)$ for transmission and $F(1)$ for reflection) is monotonically increasing with μT for (a) (b) and (d) and decreasing for (c).

Appendix B: Dependence on the momentum transfer for X-rays: arbitrary angle of incidence

For the more general case of arbitrary angle of incidence the geometric factor $F(q)$ can be obtained as follows. The asymmetry ratio $b = \gamma_0/\gamma_s$ can be expressed in terms of incidence angle α ($\gamma_0 = \cos \alpha$) and the scattering angle θ :

$$b = \frac{\cos \alpha}{\cos(\theta \pm \alpha)} \quad (\text{B1})$$

The \pm sign defines two possible scattering branches. They are shown in Fig. 5(a) and 5(b) for the transmission and reflection geometry, respectively. The beam marked by the cyan color corresponds to the upper ("+" sign in Eq. (B1) and the beam marked by the magenta color corresponds to the lower sign.

Using the reduced momentum transfer $q = \frac{Q}{2k_0} = \sin(\theta/2)$ expansion of the denominator of Eq.(B1) yields:

$$\gamma_s = (1 - 2q^2) \cos \alpha \mp \sqrt{1 - (1 - 2q^2)^2} \sin \alpha \quad (\text{B2})$$

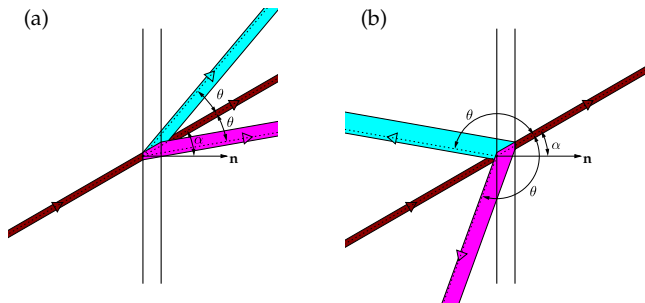


FIG. 5: Two possible scattering branches shown in (a) transmission geometry and (b) reflection geometry. The incident beam is shown with dark red color.

The expression for the geometric factor $F(q)$ given by Eqs. (23) remains valid if μT is replaced with $\mu T/\gamma_0$ and the function $f(q)$ becomes:

$$f(q) = \frac{2q(q \pm \sqrt{1 - q^2}) \tan \alpha}{1 - 2q^2 \mp 2q\sqrt{1 - q^2} \tan \alpha} \quad (\text{B3})$$

For the case $\mu T/\gamma_0 = 1$ the geometric factor for the transmission and reflection geometries is shown in Fig.6 for several different values of the incidence angle $0^\circ \leq \alpha < 90^\circ$: (a) transmission scattering geometry, and (b) reflection scattering geometry. The geometric factors corresponding to the two distinct scattering branches are shown with either solid or dashed lines.

Obviously, the two merge for $\alpha = 0^\circ$.

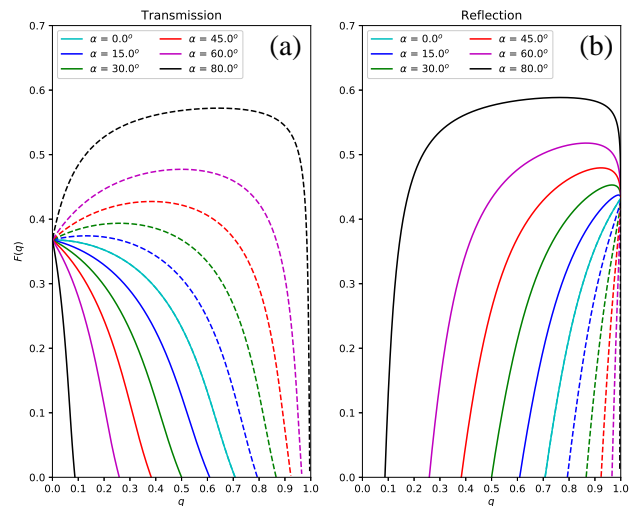


FIG. 6: Geometric factor $F(q)$ for $\mu T/\gamma_0 = 1$ plotted using several different values of the incidence angle $0^\circ \leq \alpha < 90^\circ$: (a) transmission scattering geometry, and (b) reflection scattering geometry. The geometric factors corresponding to the two distinct scattering branches are shown with either solid or dashed lines.

-
- [1] B. D. Cullity, *Elements of X-ray Diffraction*, Springer Laboratory (Addison-Wesley, Reading, Massachusetts, 1956).
- [2] W. Schülke, *Electron Dynamics by Inelastic X-ray Scattering*, vol. 7 of *Oxford series on synchrotron radiation* (Oxford University Press, Oxford; New York, 2007).
- [3] N. Stribeck, *X-ray Scattering of Soft Matter*, Springer Laboratory (Springer, Berlin Heidelberg New York, 2007).
- [4] E. N. Maslen, *International Tables for Crystallography Vol. C: Mathematical, physical and chemical tables* (Springer Netherlands, Dordrecht, 2004).
- [5] B. E. Warren and R. L. Mozzi, *Acta Cryst.* **21**, 459 (1966).
- [6] P. Fajardo, V. Honkimki, T. Buslaps, and P. Suortti, *Nucl. Instrum. Methods Phys. Res. B* **134**, 337 (1998).
- [7] O. W. Dietrich and J. Als-Nielsen, *Acta Cryst.* **18**, 184 (1965).
- [8] V. F. Sears, *Acta Cryst. A* **53**, 35 (1997).
- [9] T. M. Sabine, *International Tables for Crystallography Vol. C: Mathematical, physical and chemical tables* (Springer Netherlands, Dordrecht, 2004).
- [10] M. Berger, J. Hubbell, S. Seltzer, J. Chang, J. Coursey, R. Sukumar, D. Zucker, and K. Olsen, XCOM: Photon Cross Section Database (version 1.5) (2010), URL <http://physics.nist.gov/xcom>. National Institute of Standards and Technology, Gaithersburg, MD.
- [11] The total attenuation coefficient is often termed as total absorption coefficient. However, it should not be confused with the photoelectric absorption coefficient, since attenuation due to X-ray scattering from atoms with low atomic number can prevail at sufficiently high photon energies.